Norwegian University
of Life Sciences

Master's Thesis 2016 30 credits
Faculty of Environmental Science and Technology
Department of Ecology and Natural Resources

Assessing Accuracy of Using Unmanned Aerial System in Forest Inventory

En vurdering av nøyaktigheten ved å bruke drone til skogtaksering

Halldis Linde Lie
Forestry

Preface

This thesis is part of my Master's degree in Forestry at the Department of Ecology and Natural Resources at the Norwegian University of Life Sciences. I have been interested in forestry planning since I started studying forestry. When I got the opportunity to join a research project using unmanned aerial systems in forestry applications, it did not take me long to decide that this was something I found interesting. I am grateful for the opportunity to be part of this project. I would like to thank UMB's research fund for their financial support.

I would like to thank my main supervisor professor Terje Gobakken and co-supervisor PhD student Stefano Puliti for their help and guidance during the thesis process. You have provided me with constructive feedback, and this thesis would not have been the same without your valuable comments. I would also like to thank researcher Hans Ole Ørka for advice on the statistics.

Finally, a great thanks to my family and fellow forestry students for their good support and company.

Norwegian University of Life Sciences

Ås, May 10th 2016

Halldis Linde Lie

Abstract

Few studies have used unmanned aerial systems (UASs) in forest inventory, and few studies have compared airborne laser scanning (ALS) and UASs. In the present study, a UAS was used in a forest inventory. Based on the UAS imagery, three-dimensional (3D) point clouds were derived from a combination of structure from motion (SfM) and photogrammetric algorithms. Ground control points (GCPs) were used to increase the accuracy of the point clouds. Height and density metrics were derived from these point clouds from 33 sample plots of 500 m^2. These metrics and corresponding field measurements were used to fit linear regression models for dominant height (h_{dom}), Lorey's mean height (h_L), volume (V), basal area (G) and stem number (N). Two sets of UAS models were created, one set included spectral variables while the other did not. A third set of models were fitted using ALS data.

When comparing the UAS models with and without spectral variables, t-tests revealed that the differences were non-significant. This was also the case when the UAS models were compared to the ALS models. When compared to the ALS models, the UAS models showed a good fit in terms of adjusted R^2 (R^2_{adj}) for both h_{dom} and h_L (0.77 – 0.90). Good fits were also observed for V and G (0.73 – 0.86). With the exception of N, the relative RMSE was kept below 19.11% for all UAS models. Development class did not significantly affect the UAS models. Tree species composition indicated that the proportion of deciduous species significantly affected h_L, while the proportion of spruce significantly affected h_{dom}.

The results indicate that UAS data can be used to produce rather accurate results when used in forest inventory. Improvements on the positioning systems on the UAS could potentially make GCPs unnecessary in the future. This leads to higher efficiency and less costs, which might make UAS a more attractive tool in forestry.

Sammendrag

Få studier har brukt droner i skogtaksering, og få studier har sammenlignet flybåren laserscanning (FLS) og droner. I denne undersøkelsen ble en drone brukt til å taksere skog. Basert på bildene dronen tok ble tredimensjonale punktskyer dannet med en kombinasjon av structure from motion (SfM) og fotogrammetriske algoritmer. Passpunkt ble brukt for å øke nøyaktigheten til punktskyene. Høyde- og tetthetsvariabler ble utledet fra punktskyene av 33 prøveflater på 500 m^2. Disse variablene ble sammen med feltmålinger brukt til å lage lineære regresjonsmodeller for overhøyde (h_{dom}), middelhøyde (h_L), volum (V), grunnflate (G) og stammetall (N). To sett med dronemodeller ble laget, hvor et av settene også inneholdt fargevariabler. Et tredje sett med modeller ble laget på grunnlag av FLS-dataene.

Da dronemodellene med og uten fargevariabler ble sammenlignet kom det fram ved t-tester at differansene ikke var signifikante. Dette var også tilfellet da dronemodellene ble sammenlignet med FLS-modellene. Sammenlignet med FLS-modellene viste dronemodellene en god tilpasning ved justert R^2 (R^2_{adj}) for både h_{dom} og h_L (0.77 – 0.90). Gode tilpasninger ble også observert for modellene V og G (0.73 – 0.86). Med unntak av N ble den relative RMSE holdt under 19.11% for alle dronemodellene. Hogstklasse hadde ikke noen signifikant effekt på dronemodellene. Treslagssammensetning indikerte at andelen lauvtrær hadde en signifikant effekt på modellen h_L, mens andelen gran hadde en signifikant effekt på h_{dom}.

Resultatene indikerte at dronebilder kan bli brukt til å produsere nøyaktige resultat ved skogtaksering. Forbedringer på posisjoneringssystemene til dronene kan potensielt føre til at passpunkt blir unødvendig i fremtiden. Dette fører til større effektivitet og færre kostnader, som potensielt kan gjøre bruk av droner mer attraktivt i skogbruket.

Table of contents

1 Introduction

1.1 Background

In Norway, forest inventories have been ongoing for more than 100 years (Eid et al. 2002). The two main types of forest inventories are the national forest inventory (NFI) and the forest management inventory (FMI). The former aims to obtain data for country-level reporting and policymaking, whereas the latter aims to obtain data on forest resources at a local level for management purposes.

The first NFI in Norway started in 1919 (Anon. 2012). In Norway, this type of forest inventory is a sample survey, and important forest parameters (such as timber volume) are estimated from the collected data. The methodology has developed over the years. It started by sampling along a 10 m wide corridor, and when this proved not to be effective, circular sample plots were measured along the corridor (or sampling line) instead. The size of the sample plots gradually changed, and currently a sample size of 250 m^2 is used (Anon. 2012). Approximately 22 000 permanent sample plots are part of the NFI (Anon. 2013), and the sample plots are located all over the country. Every year one fifth of the sample plots are measured. In 2015, the 11^{th} NFI started. As opposed to the NFI, FMIs are not carried out as often.

The first records of FMIs in Norway date back to the 1870-1880s (Eid et al. 2002), although forest inventory programs were uncommon until the 1950s (Næsset 2014). As described by Næsset (2014) the early stages of FMIs in Norway were ground-based surveys to all stands of interest, identified using aerial photographs. Generally, satellite imagery are considered too coarse to retrieve details at a fine scale (Næsset 2001). Thus, for forestry applications, aerial photographs have been typically more suitable. Initially, photo interpretation and field measurements were the input for the estimation of forest attributes. In the end of the 1970s it became more common to use stereo photogrammetry in FMIs, supported by geographical information systems (Næsset & Gobakken 2015). This method was used in FMIs in Norway for almost 15 years. In the 1990s, wall-to-wall management became popular thanks to state subsidies promoting integrated forest inventories between different forest owners (Næsset 2014). This meant that large areas (i.e. entire municipalities), were inventoried as a whole. However, in 1997, digital photogrammetry was introduced to the forestry sector (Næsset 2014; Næsset & Gobakken 2015). This enabled the automation of image matching as opposed

to analogue stereo photogrammetry done with stereo plotters. Airborne laser scanning (ALS) was introduced at approximately the same time. The laser scanner (LS) emit short pulses of infrared light (Vauhkonen et al. 2014), and these pulses hit objects on the ground before they are reflected back to the sensor. The sensor registers the distance between when the pulse is emitted and when the return-pulse is registered (Næsset 1997). These distances are then used in order to calculate the height of the vegetation or terrain. ALS became a major data source, and has been used in FMIs in Norway since 2002 (Næsset & Gobakken 2015). This led to the development of the area-based approach (ABA), which uses a combination of ground reference and remotely sensed data to predict forest biophysical properties. The ABA is defined by a two-stage procedure (Næsset 2002b; White et al. 2013). At first, the ALS data is acquired for the study area, resulting in three dimensional (3D) point cloud generation. Field measurements are conducted on sample plots, and models are made for the forest biophysical properties of interest. The data is clipped, so that the data correspond to the size of the sample plots, then metrics are derived and models are developed. In the next stage, grid cells corresponding to the size of the field sample plots are laid over the stand boundary map from photointerpretation, and ALS metrics are computed for each grid cell. In order to generate the forest biophysical properties of interest, the models from the previous stage are applied to the entire study area. Once the models have been applied to the whole area, one will have estimates for each grid cell that can then be summarized to stand level (White et al. 2013).

Studies suggest that 3D data from image matching also can be used using the ABA (Gobakken et al. 2014; Næsset 2002a). Field data and remotely sensed data provide the necessary information to make a forestry plan. These forestry plans include information about the forest on the property, and the forest owner can base economic and silvicultural decisions on the information found in the forestry plan. Remotely sensed data have been widely used as auxiliary information to estimate forest biomass or volume, thanks to the ability to acquire continuous data for large areas. However, in some cases, covering small areas might also be of interest. This could be the case if one wanted to investigate an area after a storm, areas under power lines or areas pre- or post-harvest. Thus, unmanned aerial systems (UASs) could be a suitable tool in forestry, and one of the main advantages is that one gathers high-resolution imagery at the time it is needed.

UASs have been used in the military for quite some time, i.e. for surveying and warfare, but they are relatively new in other disciplines, such as forestry (Puliti et al. 2015). UAS imagery can be used in the same way as ALS. Like ALS, the point clouds characterize the canopy

structures and will therefore be useful for forest inventory purposes. Differently from ALS, which is characterized by the ability to penetrate the tree canopy and thereby enabling an accurate representation of the terrain as well as of the vegetation, UAS data will result in a model representing only the outer surface of an area (Wallace et al. 2016). However, UAS data is characterized by colour information, which can be useful when characterizing vegetation structure, such as tree species. UASs are typically optimal to map small areas, covering about 1-10 km^2 (Puliti et al. 2015; Whitehead et al. 2014). They would be ideal to use when upgrading a forestry plan for a forest property, because they are flexible, give a detailed survey of a small area and provide results rapidly (Nex & Remondino 2014).

A UAS is usually composed of a ground control system (GCS) and an unmanned aerial vehicle (UAV) (Watts et al. 2012). The GCS can be either stationary or transportable and consists of both software and hardware that are necessary to control the UAV (Colomina & Molina 2014). There are different types of UAVs, and the most common distinction between them is fixed wing, rotary wing or multirotor. They come in many different sizes, and there are many ways to classify them, often based on weight, flight endurance and altitude (Watts et al. 2012). Autopilot programs are common, although the UAV can be remotely operated if necessary. Typically, it also includes a receiver for a global navigational satellite system (GNSS) and an inertial measurement unit (IMU) (Dandois & Ellis 2010). Important factors to consider when choosing a sensor is the size and weight of it, because it will affect the UAV's performance. A result of this is that if the UAV is small, so is the sensor. Various types of sensors exist, such as multispectral, hyperspectral, thermal cameras or LS (Shahbazi et al. 2014). The aim of the survey determines which type of sensor to use.

Because of their low flying altitude (< 120 m), they are good at capturing details in the environment at a high spatial scale compared to the more conventional remote sensing equipment being used today (Whitehead & Hugenholtz 2014). This makes it possible to observe features that are too small to see from satellite or manned aircrafts (Whitehead et al. 2014). Natural disaster management, research on wildlife and aquatic ecosystems and precision agriculture are some of many applications for UASs (Shahbazi et al. 2014). A review by Colomina and Molina (2014) found that UASs can also be used for monitoring streams and rivers, coastal mapping, forest fire monitoring and tree classification. These reviews, amongst other studies, indicates the potential of using UASs for forestry applications.

1.2 Unmanned aerial systems in forestry

For forestry applications, LS and digital cameras are the most relevant UAS sensors. In several studies UAS-LS have been used in order to characterize tree or vegetation structure (Jaakkola et al. 2010; Nagai et al. 2008; Wallace et al. 2012). Due to flight regulations and battery capacity, the size and weight of the UAV are important factors to consider when planning a flight-mission. The UAVs equipped with LS are often large and heavy so that they are able to carry the necessary equipment. Nagai et al. (2008) used a large UAV (i.e. the take-off weight was about 330 kg) with multiple sensors (two cameras and one laser scanner) and the aim of the study was to create a high-resolution digital surface model (DSM). In a Finnish study Jaakkola et al. (2010) used UAS-LS for tree measurements. In their study, they found that some of the metrics derived from the 3D geometry were measured with higher precision than traditional ALS, because of the point cloud's high density. Wallace et al. (2012) also used UAS-LS to derive high-resolution point clouds for forest inventory purposes. The measurements had a high accuracy, because the increased sampling density made it more likely that the top of the tree was sampled. In another study Wallace et al. (2014) used a UAS-LS to detect the necessity of pruning of individual stems of eucalyptus in Australia. These studies indicate that UAS-LS is a suitable data source for forest inventory purposes. However, due to the weight of the equipment, it can only fly for a few minutes. Also, the power of the lasers are low, so that the vehicle has to be flown at low altitudes (Puliti et al. 2015). It also requires high technical expertise to process laser data, which in the end makes it unsuitable for forest inventory purposes. In the light of these limitations, a reasonable alternative to LS is digital cameras for 3D reconstruction through a combination of structure from motion (SfM) and photogrammetric algorithms.

Computer vision SfM and photogrammetric algorithms enable 3D point cloud generation from digital imagery (Sperlich et al. 2014). The SfM algorithms are used to derive camera locations given overlapping yet unordered images, and photogrammetric algorithms automatically locates keypoints in one image and find matches to these keypoints in other images (Dandois & Ellis 2010). Thus, the 3D geometry is generated and can be used to generate high-resolution digital surface models (DSM) (Gini et al. 2012). The flight altitude, the degree of slope in the terrain and the settings on the digital camera are some of the factors that will affect the resolution of the DSM. When subtracting an accurate ALS digital terrain model (DTM) from a high resolution UAS point cloud this results in a high resolution DSM. UAS point clouds can be used similarly to ALS point clouds.

Studies by Dandois and Ellis (2010) and Dandois and Ellis (2013) used UAS imagery and SfM to predict dominant tree height, and Lisein et al. (2013) did the same. All of these studies indicated that UAS could be used to predict tree height, and thereby there might be a potential to predict other forest biophysical properties as well. Puliti et al. (2015) used a UAS to carry out a forest inventory in Norway. SfM and photogrammetric algorithms generated point clouds from which height and density metrics were extracted. Then, these metrics were used in an ABA as independent variables to fit models for the forest biophysical properties of interest. A recent study compared UAS-LS and SfM to assess the forest structure in Tasmania, Australia (Wallace et al. 2016). The comparison indicated that UASs did not capture all variation in the understorey due to large trees that covered the small ones. Nevertheless, when using SfM most of the treetops on the test site were identified. Thus, the study demonstrated that UASs are capable of detailed 3D surveys of forests. These studies indicate that SfM is a reasonable alternative to UAS-LS, because it is possible to create high-resolution models that can be rather accurate. Less expertise is needed to operate the UAV and to process the data, compared to UAS-LS. For the mentioned reasons, SfM and photogrammetric algorithms were chosen for the current study.

1.3 Research objectives

Few studies have used UASs to carry out a forest inventory and evaluated the differences between UASs and ALS. The objectives of this study were to assess the accuracy of using a UAS in forest inventory. The forest biophysical properties of interest were dominant height (h_{dom}), Lorey's mean height (h_L), volume (V), basal area (G) and stem number (N). Because of the advantage of collecting colour information when using a digital camera as a data source, the study also evaluated the relevance of the spectral variables. The models with and without spectral variables were compared to each other. The models fitted using UAS data were compared to models fitted using ALS data. Finally, to address whether development class and tree species composition significantly affected the UAS models, dummy variables were created.

2 Materials and methods

2.1 Study area

The study area was in the municipality of Gran, in Oppland County. The elevation on the plot locations varied between approximately 130 - 570 m above sea level. The forested area consisted of mostly Norway spruce (*Picea abies* (L.) Karst.), Scots pine (*Pinus sylvestris* (L.)) and deciduous species. In most cases, spruce was observed on sites with high productivity, while pine was observed on sites with poor productivity. In the present study, Norwegian forest development classes III, IV and V were of main interest. A map of the study area is presented in Figure 1.

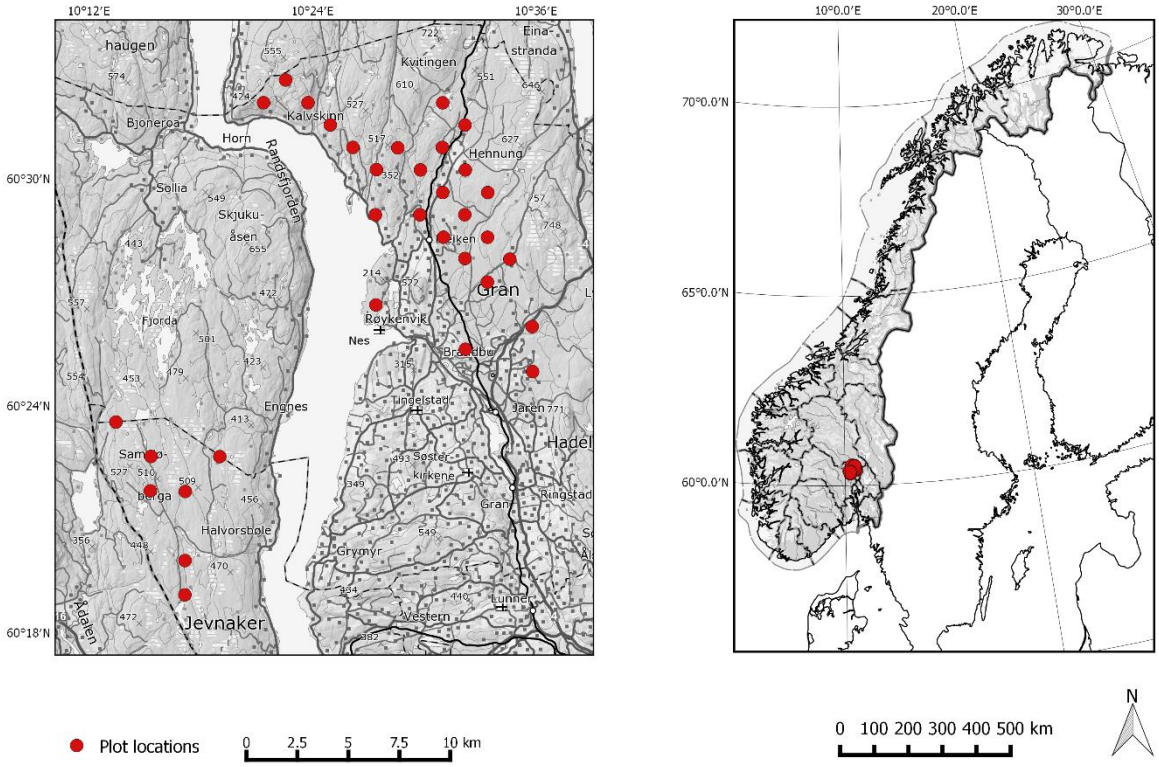

Figure 1. The map on the left show the plot locations in the study area while the map to the right indicate the location of the study area in Norway.

2.2 Field measurements

The field measurements were done during the end of August and in September 2015. Before going into the field, 33 sample plots had been placed in the study area using the geographical information system QGIS (Anon. 2016b) according to a systematic design. The sample plots were circular with a size of 500 m^2 and 1 000 m^2. The 500 m^2 plots were used for

development class III, and if the tree-density was subjectively assessed to be more than 2 000 trees per hectare. The plots of 1 000 m^2 were used for development classes IV and V. The development classes were assigned based on prior information available. Tree species was registered at each plot. The diameter at breast height (dbh) and tree position were measured on all living trees within the plot that had a dbh $\geq$ 4 cm. Tree heights were measured on sample trees, based on a probability proportional to stem basal area. Each plot had 10 sample trees. The tree height was measured using a Vertex hypsometer. The singletree volumes were estimated aided by empirical correction factors (ratio estimators), since height measurements only were available for the sample trees (both height and dbh are required in the volume equations). First a so-called base height was calculated for every tree using a base height model (Fitje & Vestjordet 1977). By means of the measured dbh and the base height, a "base volume" was calculated for each tree. In addition, for the sample trees a "true" volume was also calculated using the measured height. For each sample tree, the ratio between "true" volume and the corresponding base volume was calculated. Then, plot- and tree species-wise mean ratios (R1) were calculated. A second set of mean ratios (R2) were calculated irrespective of plot, however they were specific for tree species and three forest development classes. The plot- and species-wise mean ratios (R1) were multiplied with the base volume of each calliper tree on each respective plot to obtain an estimate of "true" volumes. However, if there were less than three sample trees of a particular species on a plot, we considered the database for the plot- and species wise mean ratio to be too small, so the species- and development class specific ratios (R2) were applied instead. Dominant height (h_{dom}) was calculated as the arithmetic mean height of the 100 largest trees per hectare according to diameter, which is a commonly used definition (Tveite 1977). Thus, h_{dom} on each plot (500 m^2) was computed as the arithmetic mean height of the five largest trees according to diameter. For each plot, Lorey's mean height (h_L) was computed as the mean height weighted by basal area. Total plot volume (V) was computed as the sum of the individual tree volumes, and these values were divided by the size of the plot in order to get volume per hectare. Basal area (G) was computed as basal area per hectare from the stem breast height diameter measurements. Stem number was computed as number of stems per hectare (N). A summary of the ground reference data are presented in Table 1.

Table 1 Summary of the ground reference data.

Characteristic*	Minimum	Maximum	Mean
h_{dom} (m)	12.2	21.9	17.39
h_L (m)	10.8	19.9	15.59
V (m^3/ha)	60.3	441.4	223.13
G (m^2/ha)	9.5	53.9	29.08
N (stems/ha)	640.0	2900.0	1609.09

* h_{dom} = dominant height, h_L = Lorey's mean height, V = volume, G = basal area, N = stem number

2.3 Remotely sensed data acquisition

ALS data was acquired in May and June 2015 as part of a large-scale acquisition covering Gran and two neighbouring municipalities. The data was collected with a Leica ALS70 sensor, which resulted in a point density of 7.45 points/m^2. The contractor (TerraTec AS, Norway) carried out the pre-processing of the ALS data. The computations included planimetric coordinates, ellipsoid height values and point cloud classification into ground and non-ground echoes according to the proprietary algorithm implemented in the TerraScan software (Anon. 2015c). A triangulated irregular network (TIN) surface was created by linear interpolation from the ground-classified points. The ALS heights were calculated above the ground.

The UAS imagery was acquired mainly in August 2015. However, some of the plots had to be re-flown at a later occasion and these flights were conducted in the middle of October and November. Table 2 show the flight acquisition dates and the plots that were flown on the specific dates. In the present study a fixed wing UAV, a senseFly eBee (Anon. 2015a), was used for the data acquisition. The UAV is fully autonomous. The eBee is a lightweight UAV, as it weighs less than 1 kg including digital camera, and it has a wingspan of 96 cm. It can be up in the air for about 50 minutes. However, wind and cold temperatures will reduce the battery capacity and thereby reduce the flight duration. In order to provide positioning the UAV had a GNSS onboard. In the current study, a Canon IXUS/ELPH multispectral digital camera was used. The camera had a focal length of 24 mm. The sensor produced three 16-megapixel images in red, green and blue wavelengths, and the resulting images had an image size of 4608 × 3456 pixels. The aspect ratio was 4:3.

Table 2 Overview of the flight acquisition dates, and the corresponding plots that were flown.

Date of flight	Plot ID
03.08.2015	2
06.08.2015	1, 26
07.08.2015	5, 6
11.08.2015	7
12.08.2015	8
13.08.2015	10, 11, 13
14.08.2015	12, 14
18.08.2015	15, 16, 17
19.08.2015	20, 22
20.08.2015	21, 23, 25
24.08.2015	18, 19
07.09.2015	3, 9
14.10.2015	27, 28, 29, 30, 32, 33, 34
15.10.2015	4
12.11.2015	24

The aviation regulations in Norway prevents a UAV lighter than 2.5 kg from being flown more than 125 m above ground, and a visual line of sight (VLOS) need to be obtained at all times (i.e. a radius of 600 m around the operator has to be upheld). The flight plans were made before going into the field using the software eMotion (Anon. 2015b). The flight altitude and amount of image overlap were the main parameters established in the planning. The altitude was set to 120 m, which resulted in a ground sampling distance of approximately 0.04 m. The low altitude results in distortions in the images, and because of these distortions a large amount of overlap is needed to correct for this (Lisein et al. 2013; Puliti et al. 2015). The image overlap was set to 90% longitudinal and 80% lateral.

In the current study, GCPs were used to georeference the point clouds. The centre of each GCP was measured in August 2015, and the total number of measured GCPs were 165. They were placed in open areas, so that they would be clearly visible from the air. Their positions were measured by differential global positioning systems (GPS) and global navigation satellite systems (GLONASS). A Topcon Legacy-E+ 40-channel dual-frequency receiver observing pseudorange and carrier phase of both GPS and GLONASS was used. The logging rate was of 2-seconds, and the centre of every GCP was measured for approximately 15 minutes. The GCPs were made of black and white checkerboard patterns, about 50 × 50 cm. Because of the time-consuming task of re-collecting these black and white checkerboards, the GCPs were eventually marked on the ground with spray paint or material available at the site. When the GCPs had been measured, the flight were carried out. The images were triggered automatically according to the pre-defined flight plan, and the eBee turned off the engine in

order to increase the stability when capturing the images. Images were captured every 3 – 4 seconds. At the end of each flight mission, the geotagged images were downloaded to the computer.

2.4 Photogrammetric processing

Agisoft PhotoScan Professional Edition 1.1.0 (64 bit) (Anon. 2014) was used to generate 3D point clouds for each of the 33 plots. The process started by importing the images. An image alignment was carried out, and the software matched keypoints in the images using SfM and photogrammetric algorithms. The GCP coordinates were imported and these were used to optimize the camera orientation. The GCPs were located manually on the images according to the markers placed on the ground. A result of this was a more accurate camera positioning, which was later used for accurate dense matching. Sparse point clouds were constructed, but as these are not useful in forestry this is followed by a dense reconstruction of the point clouds. Outliers were removed by using a mild depth filtering, reducing the level of noise in the point clouds. The dense point clouds were exported to ASCII files, with x, y, z coordinates and colour information. To obtain height above ground level, the TIN model made by the ALS data was subtracted from each point's height value.

2.5 Statistical analysis

The calculations of the statistical models were based on the 33 sample plots. For each plot, density variables ($d_1, \ldots, d_{10}$), height percentiles ($p_{10}, \ldots, p_{100}$) and coefficients of variation (cv) were calculated, for a total of 22 independent variables for both the UAS and the ALS data. When calculating the height percentiles, all points below two meters were removed from the data in order to remove rocks and underbrush from the computations. The density variables were calculated as ten equally spaced vertical layers. Six spectral variables were extracted from the plots for the UAS data. These included the mean values of the red, green and blue bands (R_m, G_m and B_m), as well as the coefficients of variation for each colour band (R_{cv}, G_{cv} and B_{cv}). Development class was assigned based on the previous operational forest inventory in the area. The forest was classified as development class III if it was young productive forest (i.e. mean height larger than approximately 7 m), class IV if mature productive forest and class V if it was old, mature forest. Tree species composition was

calculated as a percentage of the total volume of spruce, pine or deciduous species at each plot.

Multiple linear regression models were fitted for each of the forest biophysical properties of interest. Three sets of models were made for h_{dom}, h_L, *V*, *G* and *N*. Two different sets were fitted from the data collected by the UAS; one which included height and density variables, while the other one also included spectral variables. The third set was based on the height and density variables from the ALS data. Log-log transformations were used for all dependent and independent variables, which has been done in other studies using ALS (Næsset 2002b; Næsset 2004; Næsset 2007). In order to reduce the number of variables in each model, a search for the best subset was carried out using the R package leaps (Lumley & Miller 2009). Due to highly correlated variables, the variable selection was restricted to searching for models with a maximum of three variables. The reason for the strict requirement was a trial and error approach which indicated that models including more than three variables would have issues with multicollinearity. In order to avoid collinearity, the variance inflation factor (VIF) was used with a threshold of VIF < 5. This meant all variables in a model should have a VIF-value below five; otherwise, the model would be rejected. The Bayesian Information Criterion (BIC) was used to do the final variable selection. The method penalises models that include many variables. Models with the lowest BIC value were selected. A bias correction factor was used in the back-transformation of the logarithmic variables. The goodness of fit was evaluated by the adjusted R^2 (R^2_{adj}). The model assumptions that the error terms were normally distributed, had a mean equal to zero and a constant variance were checked using Shapiro-Wilkinson, t-Student and Breusch-Pagan tests, respectively.

The effects of development class and tree species composition were evaluated using t-tests. Two dummy variables were created for development class. Both were coded as zero for development class III and one for development class V. Development class IV were coded as zero for the first dummy variable and one for the second. Tree species composition was treated as a continuous variable, and three variables were created. These variables were expressed by the volume proportions of spruce, pine and deciduous species (VP_s, VP_p and VP_d). To get an indication of collinearity among the new variables added to the models, the Pearson correlation coefficients were calculated. Highly correlated variables were discarded from the models. Because the aim was to investigate whether development class and/or tree species composition had a significant effect on the UAS models, the dummy variables for development class and tree species composition were removed from the models as soon as

this was investigated. Further calculations only included the original variables (height, density and spectral variables).

Leave-one-out cross validation (LOOCV) was used to evaluate the models. Each plot acted as one observation. One plot was left out of the calculations iteratively, while the remaining plots were used to fit the models. The model's parameters were then used to predict on the left out plot. Mean differences ($\overline{D}$) and root mean square errors (RMSE) were calculated for each plot using the equations below:

$$\overline{D} = \frac{\sum_{i=1}^{n}(y_i - \hat{y}_i)}{n}$$

$$RMSE = \sqrt{\frac{\sum_{i=1}^{n}(y_i - \hat{y}_i)^2}{n}}$$

where *y* indicates the response variable of interest, $\hat{y}$ indicate the predicted value, *i* indicates the plot and *n* is the number of sample plots. For comparison purposes, the relative values of $\overline{D}$ and RMSE were calculated as a percentage of the mean observed value.

Paired t-tests on the residuals of the spectral and non-spectral models were carried out to determine whether there was a significant difference between the corresponding models. Paired t-tests were also used to test for a statistically significant difference between the models made from the UAS data and the models made from the ALS data. All tests were conducted at a 95% significance level.

3 Results

3.1 Multiple linear regression modelling

Linear models were fitted for h_{dom}, h_L, *V*, *G* and *N*, using either UAS data (i.e. with and without spectral variables) or ALS data. Most of the models included only two variables. For the UAS models without spectral variables the R^2_{adj} values for h_{dom}, h_L, *V*, *G* and *N* were of 0.88, 077, 0.84, 0.73 and 0.45, respectively. Including spectral variables in the models gave a slight increase in R^2_{adj} for all models (0.02, 0.04, 0.02 and 0) except for N, which had a slight decrease (0.01). For the ALS models the R^2_{adj} were of 0.87, 0.79, 0.91, 0.86 and 0.56 for h_{dom}, h_L, *V*, *G* and *N*, respectively. The ALS models gave larger values for R^2_{adj} when modelling *V*, *G* and *N* compared to the UAS models.

Height percentiles were present in all models except for *N*, which included two density variables instead. Only one model included the variable *cv*, which was the model h_{dom} made from the ALS data. Density variables were present in all models except h_{dom} and h_L which included spectral variables. Different spectral variables were included in the models. G_m was preferred for h_{dom} and h_L, while B_{cv} was preferred for modelling *V* and *G*. R_m was included in the model for *N*. A summary of the predictive models are presented in Table 3.

Table 3 Summary of the linear regression models for the three different datasets: UAS excluding spectral variables, UAS including spectral variables and ALS. Logarithmic transformations were used for all dependent and independent variables. The values reported for RMSE, relative RMSE (%), $\bar{D}$ and relative $\bar{D}$(%) are from the leave-one-out cross validation after back transformation.

Data	Dependent variable *	Predictive model	R^2_{adj}	RMSE	RMSE (%)	$\bar{D}$	$\bar{D}$ (%)
UAS excluding spectral variables	h_{dom} (m)	*d1 + p90*	0.88	1.02	5.85	-0.03	-0.15
	h_L (m)	*d5+p90*	0.77	1.24	7.93	-0.03	-0.20
	V (m^3/ha)	*d2+p70*	0.84	42.66	19.11	-0.67	-0.30
	G (m^2/ha)	*d1+p70*	0.73	5.54	19.03	-0.04	-0.14
	N (stems/ha)	*d1+d10*	0.45	491.65	30.55	4.58	0.28
UAS including spectral variables	h_{dom} (m)	G_m+*p80*	0.90	0.97	5.58	-0.03	-0.15
	h_L (m)	G_m+*p80*	0.81	1.13	7.24	-0.02	-0.10
	V (m^3/ha)	B_{cv}+*d1+p70*	0.86	40.65	18.22	-1.32	-0.60
	G (m^2/ha)	B_{cv}+*d2+p70*	0.73	5.56	19.11	-0.18	-0.61
	N (stems/ha)	R_m+*d1+d9*	0.44	498.70	30.99	4.63	0.29
ALS	h_{dom} (m)	*cv+d5+p20*	0.87	1.05	6.03	-0.05	-0.31
	h_L (m)	*d10+p90*	0.79	1.17	7.49	-0.03	-0.21
	V (m^3/ha)	*d1+p60*	0.91	32.68	14.51	-1.18	-0.53
	G (m^2/ha)	*d1+p50*	0.86	4.02	13.82	-0.11	-0.38
	N (stems/ha)	*d1+d9*	0.57	478.74	29.75	-1.59	-0.10

* h_{dom} = dominant height, h_L = Lorey's mean height, *V* = volume, *G* = basal area, *N* = stem number

T-tests revealed that development class had no significant effect on either of the UAS models. However, tree species composition did have a significant effect on the models h_{dom} and h_L. The Pearson correlation coefficient matrix led to the removal of the VP_p in all models, because Norway spruce and Scots pine had a large correlation coefficient (0.956). For the non-spectral UAS models VP_s had a significant effect on h_{dom} ($p = 0.003$), while the VP_d had a significant effect on h_L ($p = 0.001$). When the spectral variables were included in the model, the VP_s had a significant effect on h_{dom} ($p = 0.009$), while the VP_d had a significant effect on h_L ($p = 0.002$). An increase of one unit of VP_s led to an increase in h_{dom}, while an increase of one unit of VP_d led to a decrease in h_L.

3.2 Leave-One-Out Cross Validation

The LOOCV showed similar results for the UAS and ALS models. The RMSE values after back transformation for h_{dom}, h_L, *V*, *G* and *N* modelled from the UAS data without spectral variables were 1.02 m (5.85%), 1.24 m (7.93%), 42.66 m^3/ha (19.11%), 5.54 m^2/ha (19.03%) and 491.65 stems/ha (30.55%), respectively. Adding spectral variables to the models gave a slight decrease in relative RMSE of 0.27%, 0.69% and 0.89 % for h_{dom}, h_L and *V*, respectively. Both *G* and *N* had a slight increase in relative RMSE (0.08% and 0.44%, respectively) when spectral variables were included in the models. The RMSE values for the ALS models were 1.05 m (6.03%), 1.17 m (7.49%), 32.68 m^3/ha (14.51%), 4.02 m^2/ha (13.82%) and 478.74 stems/ha (29.75%) for h_{dom}, h_L, *V*, *G* and *N*, respectively. The largest errors were observed when predicting *N*, while the smallest errors were observed when predicting h_{dom}.

None of the $\overline{D}$s were statistically significant at a 95% confidence level for either UAS or ALS models. For the UAS models, all $\overline{D}$s reported had negative signs except for *N*, which had positive signs for the models both with and without spectral variables. The largest $\overline{D}$s were reported for *V* and *G* for the UAS models including the spectral variables, which were -0.61% and -0.60% of the ground reference values. Small relative $\overline{D}$s were observed for h_{dom} and h_L in both sets of UAS models, ranging between -0.10% and -0.20%. The relative $\overline{D}$s for the ALS models had negative signs for all models, and were in the range of -0.53 - -10%. The largest $\overline{D}$s were observed for the models *V* and *G*, similar to the UAS models. In contrast to the UAS models, the smallest $\overline{D}$ was found for the model *N*. Scatterplots of the predicted values versus

ground reference values of the forest biophysical properties of interest are found in Figure 2 and Figure 3 for UAS- and ALS models, respectively.

Paired t-tests revealed that there were no significant differences between the UAS models with and without spectral variables, and there were no significant differences when comparing the ALS models to the UAS models. At log-scale, the residual analysis revealed that none of the model assumptions were violated at a 95% significance level. The error terms were normally distributed ($p \geq 0.071$), had a mean equal to zero ($p = 1$) and they had a constant variance ($p \geq 0.279$).

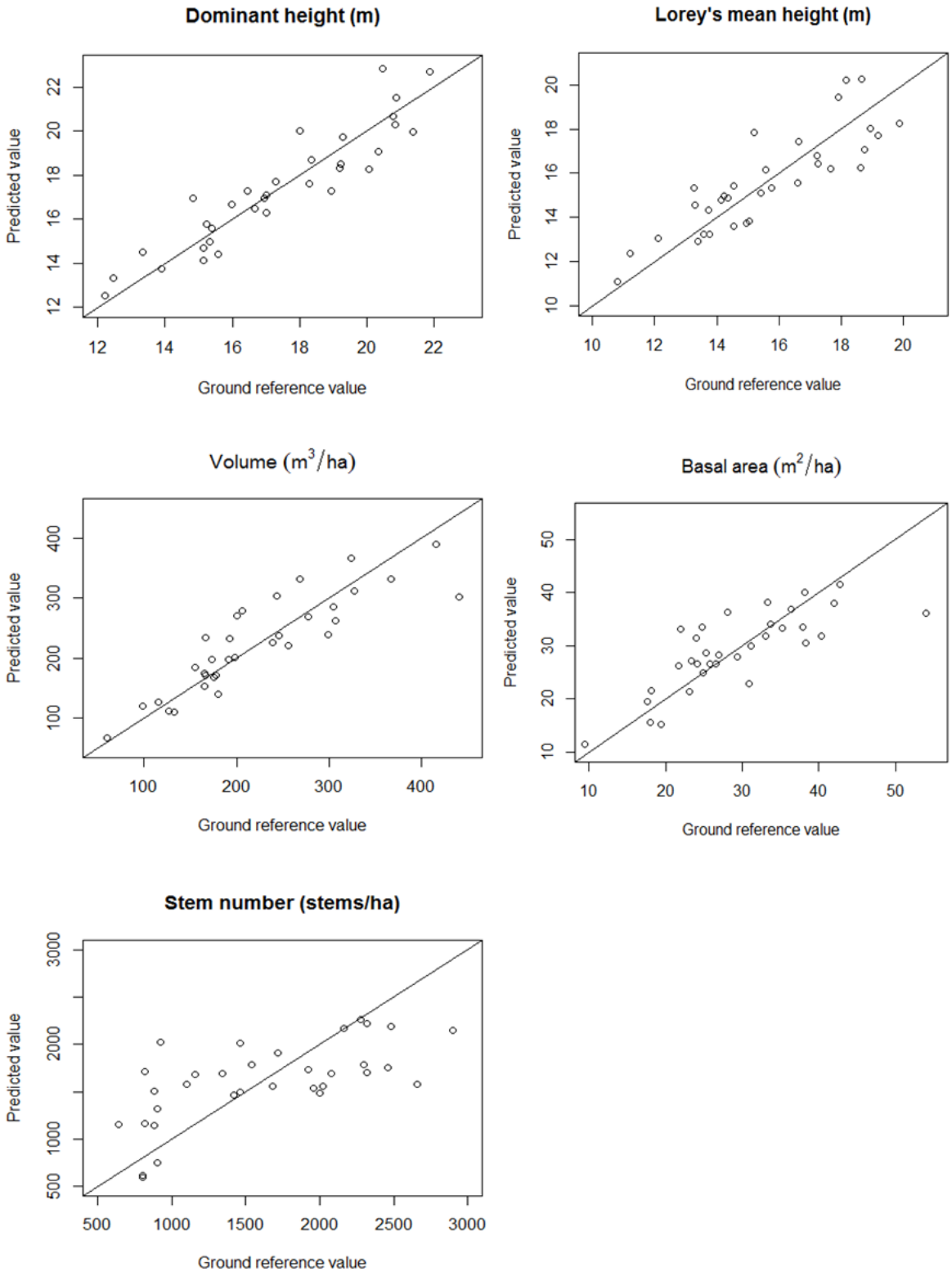

Figure 2 Scatterplots showing the predicted versus ground reference values for the forest biophysical properties of interest. The plots are based on the cross validated values from the UAS data without spectra variables.

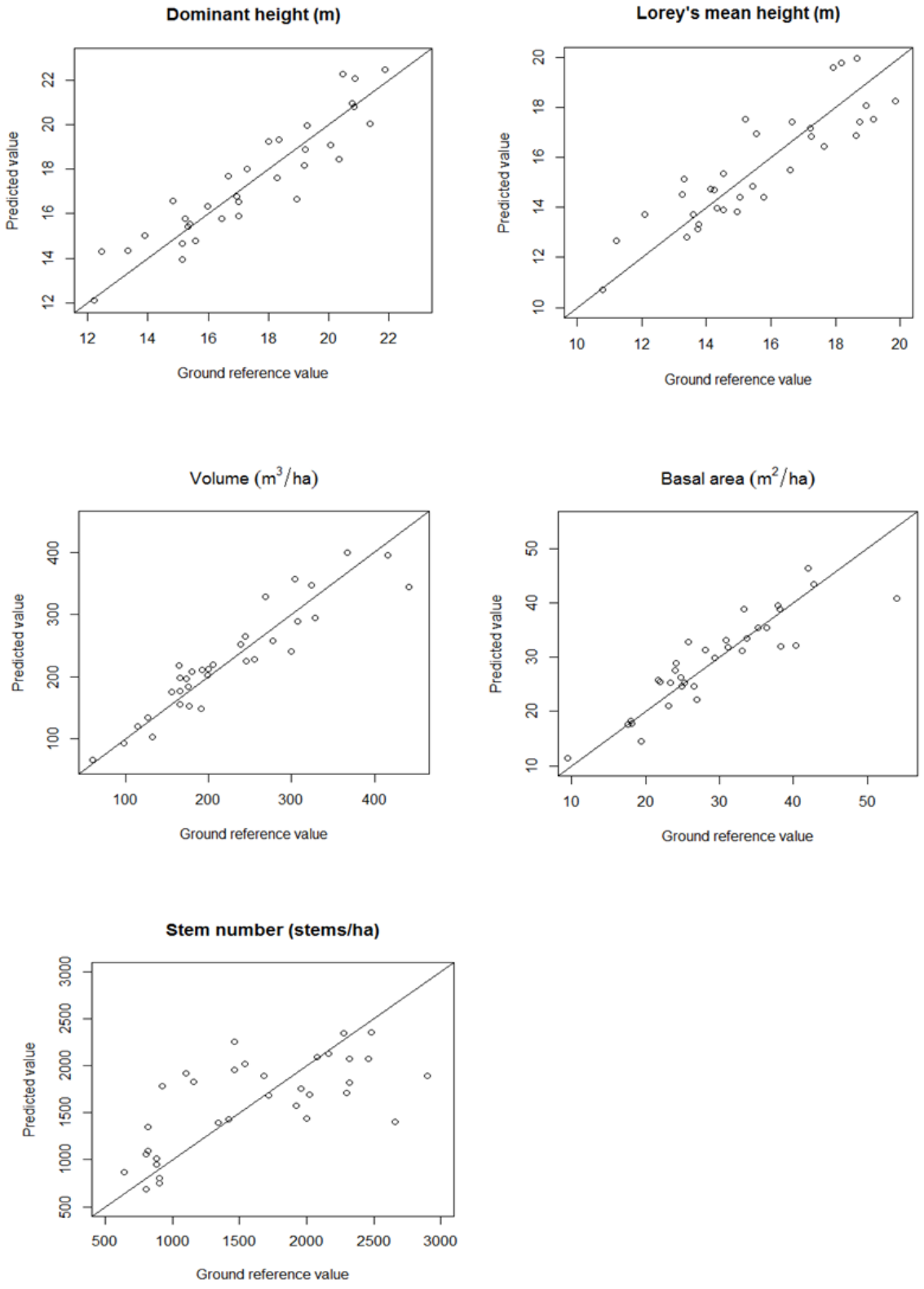

Figure 3 Scatterplots showing the predicted versus ground reference values for the forest biophysical properties of interest, based on the cross-validated ALS data

4 Discussion

4.1 Accuracy assessment

Density variables (d_1, d_2, d_5 and d_{10}) were present in all UAS models without spectral variables. For the models including spectral variables, density variables (d_1, d_2 and d_9) were present in the models *V*, *G* and *N*. In both cases, *N* included two density variables. In the study by Puliti et al. (2015), the density variables were either small (d_0) or large (d_7 and d_9). Similarly, two density variables were selected for the model *N* (d_0 and d_9). In the current study, height percentiles were present in all UAS models, except for *N*. The height percentiles present were all high, namely p_{70}, p_{80} and p_{90}. Puliti et al. (2015) reported a wider range of height percentiles (p_{20}, p_{30}, p_{50}, p_{80} and p_{100}) than the current study. In the models h_{dom} and h_L, the density variables were replaced with the spectral variable G_m, similar in both studies. Unlike the current study, neither the blue nor the red bands were represented in the models reported in Puliti et al. (2015). This might be due to the time when the imagery was acquired. In their study, the imagery was acquired in a couple of days in November and December, while the present study acquired the imagery mainly in August.

Except for *N*, all models showed a rather good fit as the R^2_{adj} ranged from 0.73 – 0.88 for the UAS models without spectral variables and 0.73 – 0.90 when including spectral variables. For h_{dom} and h_L, the R^2_{adj} was similar for both sets of UAS models. For the models without spectral variables, Puliti et al. (2015) reported R^2_{adj} of 0.96, 0.68, 085, 0.60 and 0.57 for h_{dom}, h_L, *V*, *G* and *N*, respectively. When spectral variables were included in the models, the R^2_{adj} reported were 0.97, 0.71 and 0.60 for h_{dom}, h_L and *N*, respectively. They revealed larger R^2_{adj} when predicting h_{dom} and *N*, but the other values were in the same range as the current study. The study was conducted in boreal coniferous forests, similar to the present study. However, it should be noted that in the current study log-log transformations were used on all variables, as opposed to their study that used log-log transformations on h_L, *V* and *N* exclusively. Previous research have used UAS data to model h_{dom}. A study conducted by Dandois and Ellis (2010) revealed an R^2_{adj} of 0.80 and 0.53 for their two study sites. Another study conducted by Dandois and Ellis (2013) revealed an R^2 varying between 0.07 and 0.84. The R^2 reported in these two studies are consistently smaller than the values reported in the present study. Lisein et al. (2013) also used UAS data to predict h_{dom}, and reported an R^2_{adj} of 0.82 at stand level. At the individual tree level, their results revealed an R^2_{adj} of 0.91. These results are similar to the present study. However, in their studies Dandois and Ellis (2010); Dandois and

Ellis (2013) and Lisein et al. (2013) used different flight altitude, cameras and camera settings, differing number of GCPs and various software to process the data.

The ALS models also showed a good fit, as the R^2_{adj} were in the range of 0.79 – 0.91 (excluding *N*). The h_{dom} model revealed a smaller R^2_{adj} than the corresponding UAS models (a difference of 0.03 and 0.01 with and without spectral variables, respectively). Both *V* and *G* had larger R^2_{adj} when using ALS data. The differences in R^2_{adj} were 0.13 for the model *G* and 0.07 and 0.05 for non-spectral and spectral *V*-models, respectively. When modelling *N*, the ALS model had a larger R^2_{adj} (0.57) than the corresponding UAS models (0.45 and 0.44). Numerous studies have used ALS to predict forest biophysical properties in coniferous forests. Næsset (2002b) used a stratification that divided the forested areas into strata based on age and site productivity. The study revealed R^2 ranging from 0.65 – 0.86 in mature forest on poor sites and 0.50 – 0.85 in mature forest on good sites. Another study conducted by Næsset (2004) reported R^2 ranging from 0.77 – 0.91 for mature forest on poor sites and 0.60 – 0.85 for mature forest on good sites. The R^2 values reported in these two studies are in the same range as the R^2_{adj} reported for the UAS models in the current study. However, Næsset's studies revealed larger values when predicting *N* (0.50 – 0.68 and 0.60 – 0.81). Gobakken et al. (2014) compared image matching and ALS. They modelled h_{dom}, h_L, *V*, *G* and *N* for mature forest on poor and good sites. For mature forest on poor sites, Gobakken et al. (2014) reported R^2 of approximately 0.70 – 0.90, and for mature forest on good sites the R^2 were approximately 0.60 – 0.90 when using ALS data. In the current study, the UAS model *N* had a smaller R^2_{adj} than the corresponding ALS model.

With the exception of *N*, the errors in terms of relative RMSE were kept below 19.11% for all UAS models. H_{dom} proved to be the most accurate model. For the model without spectral variables the RMSE was 1.02 m (5.85%) and including spectral variables the RMSE was 0.97 m (5.58%). Puliti et al. (2015) revealed more accurate models for h_{dom}. Their study reported a RMSE of 0.72 m (3.64%) without spectral variables and 0.69 m (3.48%) including spectral variables. In contrast to the current study, which used two independent variables in the models, Puliti et al. (2015) used three and four independent variables in the models. When predicting h_{dom}, both studies by Dandois and Ellis reported larger RMSEs than the current study. Dandois and Ellis (2010) reported RMSEs of 2.9 m and 4.2 m for their two study sites, while Dandois and Ellis (2013) revealed RMSEs varying between 3.2 and 6.8 m. Lisein et al. (2013) reported a RMSE of 1.65 m (8.4%) at a stand level. However, they reported a RMSE of 1.04 m (4.7%) at an individual tree level, similar to the results in the current study. For the

model h_L, the current study reported smaller values for RMSE (1.24 m and 1.13 m) and relative RMSE (7.93% and 7.24%), than Puliti et al. (2015). In their study, when excluding spectral variables, the reported RMSE were 1.55 m (13.66%). This was slightly reduced when including spectral variables (1.51 m; 13.28%). When modelling *V* and *G*, the current study revealed relative RMSEs of roughly 19%, both with and without spectral variables, while Puliti et al. (2015) reported smaller values. For *V*, they reported values of 14.95%, while they reported values for *G* were 15.38%. Neither of these models included spectral variables. When modelling *N*, the current study revealed relative RMSEs of 30.55% (491.65 stems/ha) and 30.99% (498.70 stems/ha) for the models with and without spectral variables, respectively. The scatterplot in Figure 2 show an overestimation of small values and an underestimation of large values for *N*. Puliti et al. (2015) also reported an underestimation of large values for *N*, and reported errors of 39.24% (538.31 stems/ha) and 38.57% (529.03 stems/ha) with and without spectral variables, respectively.

In the current study, there were no statistically significant differences between the UAS- and ALS models. In terms of relative RMSE, the UAS model h_{dom} (without spectral variables) revealed a smaller relative RMSE than the corresponding ALS model (5.85% vs. 6.03%). Furthermore, both h_{dom} and h_L revealed smaller relative RMSEs for the UAS models including spectral variables than the corresponding ALS models (a difference of 0.45% and 0.25%, respectively). When comparing the model *V*, the UAS- and ALS models had a difference in relative RMSE of 4.6% (without spectral variables) and 3.7% (including spectral variables). When comparing the model *G*, this difference was 5.2% (without spectral variables) and 5.3% (including spectral variables). Differences in relative RMSE of 0.8% and 1.24% were observed when comparing *N*. Although the differences were non-significant, it seems like the largest differences in accuracy between UAS and ALS can be found when modelling *V* and *G*. Previous research has compared ALS and photogrammetric methods for predicting forest biophysical properties. For image matching, Gobakken et al. (2014) reported relative RMSEs varying between 6.6 - 28.6% and 9.2 – 43.7% for mature forest on poor and good sites, respectively. The values reported for ALS were smaller, 6.5 – 20.6% and 7.5 – 35.1% for mature forest on poor and good sites, respectively. These RMSE values are consistent with the current study, which ranged from 5.85 – 30.55% and 5.58 – 30.99% for the UAS models with and without spectral variables.

The $\overline{D}$s were not significantly different from zero. The relative $\overline{D}$s reported in this study were small, and the largest relative $\overline{D}$ was -0.61% of the ground reference value. The UAS models

without spectral variables had $\overline{D}$s in the range of -0.67 – 4.58 (-0.30 - 0.28%), and when spectral variables were included, the range was -1.32 – 4.63 (-0.61 - 0.29%). The negative signs reported for all $\overline{D}$s (except for *N*) in the UAS models, indicated that there was an overall tendency of overestimation. However, the positive sign in the *N* models indicated that *N* was underestimated, as stated earlier (Figure 2). Similar to the current study, Puliti et al. (2015) reported relative $\overline{D}$s of 0.05, 0.13, 0.21, 0.09 and -0.60% for h_{dom}, h_L, *V*, *G* and *N* (without spectral variables), respectively. In the three models that included spectral variables (h_{dom}, h_L and *N*) the $\overline{D}$s were 0.04, 0.03 and -0.36%. In contrast to the current study, Puliti reported positive signs for all models except for *N*, which translates to underestimation of the predicted values.

For the ALS models the $\overline{D}$s ranged from -1.59 to -0.03 (-0.53 to -0.10%). Compared to the ALS models, smaller relative $\overline{D}$s were observed for the UAS models h_{dom} and h_L, both with and without spectral variables. This was also the case for *V* and *G* without spectral variables. However, the relative $\overline{D}$ was smaller for the ALS model *N*. Næsset (2002b) reported $\overline{D}$s in the range of -0.01 - 6 for mature forest on poor sites and 0.01 - 38 for mature forest on good sites. The largest $\overline{D}$s were reported for *N*, similar to the current study. The $\overline{D}$s reported in Næsset (2004) were in the range of -0.03 – 6 and 0 – 1 for mature forest on poor and good sites, respectively. Both of these studies used LOOCV, similar to the current study. However, no trees below 10 cm were callipered in the mature forest study sites in Næsset's studies, while all trees above 4 cm were callipered in the present study. In addition, the plot sizes in his two studies were 200 and 232.9 m^2, which is less than half the size of the plot size in the present study. Large plots are expected to give more accurate results than small plots (Gobakken & Næsset 2008; Gobakken & Næsset 2009). Thus, this might explain some of the differences in results.

4.2 Spectral variables

There were no statistically significant differences between the UAS models with and without spectral variables. Thus, the importance of spectral variables can be questioned. As stated earlier, the goodness of fit had a slight increase when adding spectral variables to the models (0.02, 0.04, 0.02, 0 and -0.01 for h_{dom}, h_L, *V*, *G* and *N*, respectively). Puliti et al. (2015) reported an increase in R^2_{adj} of 0.01, 0.03 and 0.03 for the models that included spectral variables (h_{dom}, h_L and *N*). Furthermore, the spectral variables only led to a slight decrease in

relative RMSE for the models h_{dom}, h_L and V (0.27, 0.69 and 0.89%, respectively), while G and N had an increase in relative RMSE (-0.08 and -0.44%). This is consistent with previous research which also reported a decrease in relative RMSE for the models h_{dom} and h_L, in addition to an increase in relative RMSE for the model N (Puliti et al. 2015). The imagery in the current study was collected in August, October and November, and the variation in light and atmospheric conditions during the different flight acquisition dates were probably not optimal for assessing the viability of the spectral data. Ideally, all flights should be conducted within the same timeframe. It is likely that because most of the imagery in the current study was collected during the vegetative season it was better than the data Puliti et al. (2015) used in their study in Våler. However, there will still be problems with heterogeneity of the light and atmospheric conditions that increases the level of noise in the spectral data. Eventually, the use of band rations could potentially result in more homogenous information and possibly better results.

4.3 Development class and tree species composition

Development class had no significant effect on the UAS models. Thus, there were no significant differences between young productive forest and mature productive forests. VP_s had a significant effect on h_{dom}, indicating that an increase of one unit of VP_s led to an increase in h_{dom}. Norway spruce can potentially grow taller than deciduous species found in Norway, therefore it seems reliable that an increase of VP_s per hectare will increase h_{dom}. The addition of VP_d in the h_L model led to a significant effect on h_L, indicating that an increase of one unit of VP_d led to a decrease in h_L. Thus, if there is a large amount of deciduous species in a forest, the models indicated that the mean height in the forest would be lower than in for example a forest consisting of conifers like Norway spruce and Scots pine.

4.4 General considerations

GCPs were used in order to increase the accuracy of the 3D point clouds generated from the UAS imagery. As indicated in the methods section, the GCPs were made of black and white checkerboard patterns as well as objects found in nature. The centres of the GCPs were located in the software Agisoft PhotoScan. On some of the images, the GCPs were hard to locate. Often, this was due to low contrasts in the images. In addition, some of the rocks and

sticks that were used might have been too small, which made them hard to find. Fog and low cloud cover also made the GCPs hard to locate. Other factors of importance are the distortions on the sides of the images, and shadows cast by the trees. Measuring GCPs was a time-consuming task, and in order to improve the efficiency of the data collection an option could have been to reduce the number of GCPs. However, this will probably affect the accuracy of the georeferenced point cloud. The eBee has a positional accuracy down to 3 cm when GCPs are measured, but without GCPs the positional accuracy varies between 1-5 m (Anon. 2016b). However, the senseFly eBee RTK (Anon. 2016a) is reported to have a positional accuracy down to 3 cm without using GCPs. This will lead to a more efficient data collection.

Both aviation regulations and battery capacity affect the size of the study area. If the battery capacity improves, it will lead to an increase in flight duration and larger areas being covered in one flight. Changes in the aviation regulations in Norway may occur, which can affect the regulations concerning the VLOS. Today, the VLOS is set to a radius of 600 meters around the operator and a maximum flight altitude of 125 m (for small UASs). If this either increases or is removed from the regulations, each flight can cover larger areas and alternatively it can cover larger areas with sloping terrain, which makes it difficult to maintain the VLOS. If the size of the study area can be increased, this may make UASs more attractive for data collection in forestry.

5 Conclusions

When compared to ALS, the results of the current study indicate that UAS and photogrammetric data can be used to accurately model forest biophysical properties. This indicates that UAS can be a substitute or a supplement for ALS, given that an accurate DTM of the area exist. UAS may be a viable tool for various forestry applications such as a forest inventory. The high spatial resolution of the imagery collected by the UAS can potentially be used for pre- and post-harvest surveys, or to map windfallen trees or other forms of natural disturbances. Both technology and software are rapidly evolving, and UASs are now available to a wide audience. As it is today in forestry, UASs are mostly used for research purposes, although there is an increasing number of companies using them for commercial purposes as well. The rapid changes might lead to cheaper equipment with improved free license software, making UASs more attractive for people outside the research community.

6 References

Anon. (2012). *Landsskogtakseringens takstsystemer (National forest inventory methods)*. Ås: Norwegian Forest and Landscape Institute. Available at: http://www.skogoglandskap.no/fagartikler/2007/1197454382.24 (accessed: 10.03.2016).

Anon. (2013). *Fakta om Landsskogtakseringen (Facts about the national forest inventory)*. Available at: http://www.skogoglandskap.no/artikler/2013/fakta_om_landsskogtakseringen (accessed: 17.03.2016).

Anon. (2014). *Agisoft Photoscan User Manual*. Available at: http://www.agisoft.com/pdf/photoscan-pro_1_1_en.pdf (accessed: 02.03.2016).

Anon. (2015a). *eBee Extended User Manual*. Available at: https://www.sensefly.com/fileadmin/user_upload/sensefly/documents/manuals/Extended_User_Manual_eBee_and_eBee_Ag_v16.pdf (accessed: 04.03.2016).

Anon. (2015b). *eMotion: Release Notes*. Available at: https://www.sensefly.com/fileadmin/user_upload/sensefly/documents/release_notes/Release_Notes_2.4.5.pdf (accessed: 08.03.2016).

Anon. (2015c). *TerraScan User's Guide*. Available at: https://www.terrasolid.com/download/tscan.pdf (accessed: 02.03.2016).

Anon. (2016a). *eBee RTK: the survey-grade mapping drone*. Available at: https://www.sensefly.com/fileadmin/user_upload/sensefly/documents/brochures/eBee_RTK_en.pdf (accessed: 16.03.2016).

Anon. (2016b). *QGIS Geographic Information System. Open Source Geospatial Foundation Project*. Available at: http://www.qgis.org/en/site/ (accessed: 23.02.2016).

Colomina, I. & Molina, P. (2014). Unmanned aerial systems for photogrammetry and remote sensing: A review. *ISPRS Journal of Photogrammetry and Remote Sensing*, 92: 79-97.

Dandois, J. P. & Ellis, E. C. (2010). Remote sensing of vegetation structure using computer vision. *Remote Sensing*, 2: 1157-1176.

Dandois, J. P. & Ellis, E. C. (2013). High spatial resolution three-dimensional mapping of vegetation spectral dynamics using computer vision. *Remote Sensing of Environment*, 136: 259-276.

Eid, T., Fitje, A. & Hoen, H. F. (2002). *Økonomi og planlegging : teknisk fagskole : fordypningsområde skogbruk*. Oslo: Gan. 205 pp.

Fitje, A. & Vestjordet, E. (1977). Bestandshøydekurver og nye tarifftabeller for gran (Stand height curves and new tariff tables for Norway spruce): Norwegian Forest and Research Institute. 68 pp.

Gini, R., Passoni, D., Pinto, L. & Sona, G. (2012). Aerial images from an UAV system: 3d modeling and tree species classification in a park area. *International Archives of the Photogrammetry, Remote Sensing and Spatial Information Sciences*, 39 (B1): 361-366.

Gobakken, T. & Næsset, E. (2008). Assessing effects of laser point density, ground sampling intensity, and field sample plot size on biophysical stand properties derived from airborne laser scanner data. *Canadian Journal of Forest Research*, 38 (5): 1095-1109.

Gobakken, T. & Næsset, E. (2009). Assessing effects of positioning errors and sample plot size on biophysical stand properties derived from airborne laser scanner data. *Canadian Journal of Forest Research*, 39 (5): 1036-1052.

Gobakken, T., Bollandsås, O. M. & Næsset, E. (2014). Comparing biophysical forest characteristics estimated from photogrammetric matching of aerial images and airborne laser scanning data. *Scandinavian Journal of Forest Research*, 30 (1): 73-86.

Jaakkola, A., Hyyppä, J., Kukko, A., Yu, X., Kaartinen, H., Lehtomäki, M. & Lin, Y. (2010). A low-cost multi-sensoral mobile mapping system and its feasibility for tree measurements. *ISPRS journal of Photogrammetry and Remote Sensing*, 65 (6): 514-522.

Lisein, J., Pierrot-Deseilligny, M., Bonnet, S. & Lejeune, P. (2013). A photogrammetric workflow for the creation of a forest canopy height model from small unmanned aerial system imagery. *Forests*, 4 (4): 922-944.

Lumley, T. & Miller, A. (2009). *Package "Leaps": Regression subset selection*. Available at: https://cran.r-project.org/web/packages/leaps/leaps.pdf (accessed: 12.04.2016).

Nagai, M., Chen, T., Ahmed, A. & Shibasaki, R. (2008). UAV borne mapping by multi sensor integration. *The International Archives of the Photogrammetry, Remote Sensing and Spatial Information Sciences*, 37: 1215-1221.
Nex, F. & Remondino, F. (2014). UAV for 3D mapping applications: a review. *Applied Geomatics*, 6 (1): 1-15.
Næsset, E. (1997). Determination of mean tree height of forest stands using airborne laser scanner data. *ISPRS Journal of Photogrammetry and Remote Sensing*, 52 (2): 49-56.
Næsset, E. (2001). Ressursregistrering med flybåren laser-skanner - snart virkelighet (Resource inventory with airborne laser scanner: soon a reality). *Norsk Skogbruk*, 47 (5): 20-23.
Næsset, E. (2002a). Determination of mean tree height of forest stands by digital photogrammetry. *Scandinavian Journal of Forest Research*, 17 (5): 446-459.
Næsset, E. (2002b). Predicting forest stand characteristics with airborne scanning laser using a practical two-stage procedure and field data. *Remote Sensing of Environment*, 80 (1): 88-99.
Næsset, E. (2004). Practical large-scale forest stand inventory using a small-footprint airborne scanning laser. *Scandinavian Journal of Forest Research*, 19 (2): 164-179.
Næsset, E. (2007). Airborne laser scanning as a method in operational forest inventory: Status of accuracy assessments accomplished in Scandinavia. *Scandinavian Journal of Forest Research*, 22 (5): 433-442.
Næsset, E. (2014). Area-based inventory in Norway - from innovation to an operational reality In Maltamo, M., Næsset, E. & Vauhkonen, J. (eds) vol. 27 *Forestry applications of airborne laser scanning: concepts and case studies*, p. 464. Dordrecht: Springer.
Næsset, E. & Gobakken, T. (2015). Ressursregistrering og skogbruksplanlegging - en renessanse for flybildene? (Resource inventory and forestry planning - a renaissance for aerial photographs?). *Norsk Skogbruk* (2): 34-37.
Puliti, S., Ørka, H. O., Gobakken, T. & Næsset, E. (2015). Inventory of small forest areas using an unmanned aerial system. *Remote Sensing*, 7 (8): 9632-9654.
Shahbazi, M., Théau, J. & Ménard, P. (2014). Recent applications of unmanned aerial imagery in natural resource management. *GIScience & Remote Sensing*, 51 (4): 339-365.
Sperlich, M., Kattenborn, T., Koch, B. & Kattenborn, G. (2014). *Potential of unmanned aerial vehicle based photogrammetric point clouds for automatic single tree detection*. Available at: https://www.researchgate.net/profile/Teja_Kattenborn/publication/261643648_Potential_of_Unmanned_Aerial_Vehicle_Based_Photogrammetric_Point_Clouds_for_Automatic_Single_Tree_Detection/links/0c960534ea7ab61ef7000000.pdf (accessed: 19.04.2016).
Tveite, B. (1977). *Bonitetskurver for gran (Site-index curves for Norway spruce (Picea abies (L.) Karst.))*, vol. 33: Norsk institutt for skogforskning. 1-84 pp.
Vauhkonen, J., Maltamo, M., McRoberts, R. E. & Næsset, E. (2014). Introduction to forestry applications of airborne laser scanning. In Maltamo, M., Næsset, E. & Vauhkonen, J. (eds) Managing Forest Ecosystems, vol. 27 *Forestry Applications of Airborne Laser Scanning: Concepts and Case Studies*, pp. 1-16. Dordrecht: Springer.
Wallace, L., Lucieer, A., Watson, C. & Turner, D. (2012). Development of a UAV-LiDAR system with application to forest inventory. *Remote Sensing*, 4 (6): 1519-1543.
Wallace, L., Watson, C. & Lucieer, A. (2014). Detecting pruning of individual stems using airborne laser scanning data captured from an unmanned aerial vehicle. *International Journal of Applied Earth Observation and Geoinformation*, 30: 76-85.
Wallace, L., Lucieer, A., Malenovský, Z., Turner, D. & Vopěnka, P. (2016). Assessment of forest structure using two UAV techniques: A comparison of airborne laser scanning and structure from motion (SfM) point clouds. *Forests*, 7 (3): 62.
Watts, A. C., Ambrosia, V. G. & Hinkley, E. A. (2012). Unmanned aircraft systems in remote sensing and scientific research: Classification and considerations of use. *Remote Sensing*, 4 (6): 1671-1692.
White, J. C., Wulder, M. A., Vastaranta, M., Coops, N. C., Pitt, D. & Woods, M. (2013). The utility of image-based point clouds for forest inventory: A comparison with airborne laser scanning. *Forests*, 4 (3): 518-536.

Whitehead, K. & Hugenholtz, C. H. (2014). Remote sensing of the environment with small unmanned aircraft systems (UASs), part 1: a review of progress and challenges. *Journal of Unmanned Vehicle Systems*, 02 (03): 69-85.

Whitehead, K., Hugenholtz, C. H., Myshak, S., Brown, O., LeClair, A., Tamminga, A., Barchyn, T. E., Moorman, B. & Eaton, B. (2014). Remote sensing of the environment with small unmanned aircraft systems (UASs), part 2: scientific and commercial applications. *Journal of Unmanned Vehicle Systems*, 02 (03): 86-102.

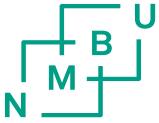

Norwegian University
of Life Sciences

Postboks 5003
NO-1432 Ås, Norway
+47 67 23 00 00
www.nmbu.no